Ultra-short laser-induced high aspect ratio densification in porous glass

Tatiana Itina, Roman Zakoldaev, Maxim Sergeev, Hongfeng Ma, Sergey I Kudryashov, Oleg S Medvedev, Vadim P Veiko

Research Article | Vol. 9, No. 11 / 1 November 2019 / Optical Materials Express 4379
Optical Materials EXPRESS

Ultra-short laser-induced high aspect ratio densification in porous glass

Tatiana E. Itina,[1,2,*] Roman A. Zakoldaev,[2] Maxim M. Sergeev,[2] Hongfeng Ma,[1] Sergey I. Kudryashov,[2,3] Oleg S. Medvedev,[4] and Vadim P. Veiko[2]

[1]Laboratoire Hubert Curien, UMR CNRS 5516/UJM/Univ. Lyon, Bat. F, 18 rue du Pr. Benoit Lauras, 42000 Saint-Etienne, France
[2]ITMO University, 49 Kronverkskiy prt, 197101 Saint-Petersburg, Russia
[3]Lebedev Physical Institute, 53 Leninsky prt, 119991 Moscow, Russia
[4]Saint-Petersburg State University, Research Park, IRC for Nanotechnology, 198504 Saint-Petersburg, Russia
*tatiana.itina@univ-st-etienne.fr

Abstract: Multiple ultra-short laser irradiation enabling direct writing of high aspect ratio barriers is used for structuring of nanoporous glass. Shape and morphology of laser-modified regions are examined, and high aspect ratio laser-induced material densification is founded. Experimental results are analyzed by modeling describing laser propagation, non-linear ionization and thermal effects. The role of laser focusing, laser energy and pulse number are examined. Several regimes are distinguished. Particularly, high-aspect ratio densified zones are obtained for the numerical aperture of 0.25, whereas either more symmetric densified regions or spherical cavities are shown to be formed for numerical aperture of 0.4. The resulting laser irradiation conditions required for deep and prolonged densification are explained by a lower ionization rate, leading to the under-critical free electron plasma density, longer filamentation and pulse-to-pulse elongation effects. Furthermore, filling of the porous glass with water is demonstrated to particularly extend the length of the densified region in depth. The presented study provides insights facilitating laser-based fabrication of barriers, membrane and patterns suitable for the environmental gas-phase analysis.

1. Introduction

Laser-induced formation of complex three-dimensional structures inside transparent optical materials [1–4] has attracted tremendous attention during last decade due to numerous emerging applications in photonics [1,5], optics [6], as well as in many other industrial [7] and medical fields [8]. In particular, such structures as periodic volume nanogratings [9], lattices [10], voids [11] and channels [12] were fabricated by either single or multiple ultra-short laser irradiation. Because of multi-photon absorption, ultra-short laser treatment can be strongly confined facilitating the control over laser energy deposition. Additionally, by changing the deposited energy density, the induced material modifications range from structural transitions, such as defects formation and densification [13], to cavitation [9], cracks or even long channel formation [14–16].

Ultra-short treatment of optical materials was shown to be particularly promising in multi-pulse regime, both for surface structuring [17–20] and for material treatment in volume [21–25]. These experiments demonstrated that the size of the laser-affected zone increases with laser pulse energy if laser repetition rate becomes larger than a certain critical value. This effect strongly depends on both absorbed laser energy and absorption volume determining the following heat diffusion from each individual pulse [23,26,27]. Despite the fact that at room temperature optical materials have much lower thermal expansion coefficients than metals, thermo-mechanical effects commonly also enter in the play. While appearing long after the laser pulse, these effects are known to play a

#367834 https://doi.org/10.1364/OME.9.004379
Journal © 2019 Received 16 May 2019; revised 11 Jul 2019; accepted 28 Jul 2019; published 18 Oct 2019

Optical Materials EXPRESS

significant role at either reduced or zero laser scanning speed [19]. The non-linear absorptivity of glasses, such as foturan, was shown to depend on both laser repetition rate and laser pulse energy [2,23]. Aberration corrections were also found to be crucial for deep three-dimensional laser machining [28]. Additionally, several effects of scanning speed and laser focusing conditions were discussed [23,27,29].

Despite numerous results obtained for fused silica and other glasses, porous glass (PG) is still much less studied than more common ones. Nevertheless, PG has a huge potential in laser-based fabrication of photonics components, as well as various barriers for integrated multi-purpose fluidic elements (Fig. 1, a). A variety of structures was already produced in PG by using different lasers, ranging from continuous wave (CW) to short and ultra-short ones. Depending on the laser treatment regime, localized densification, voids or channels could be obtained by scanning multi-pulse femtosecond laser irradiation [15]. Furthermore, PG with its high absorption capability is very efficient for capturing reagents, analytes ([30,31], bio components [32] or digital information [33]. Among various effects of ultra-short laser pulses, their capacity to considerably reduce pore size and induce glass structural modifications are particularly promising since locally densified regions can be used as barriers. Such barriers with controlled permeability were efficiently produced in PG through its local bulk density modification by direct femtosecond laser writing [34].

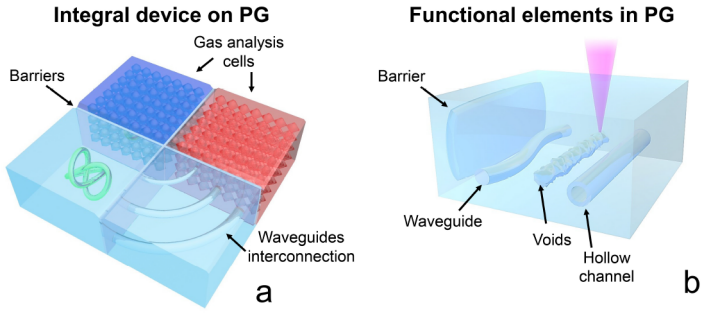

Fig. 1. Geometrically and morphologically changeable modified regions produced by femtosecond laser pulses: molecular barriers, waveguides, isolated nanoporous cells (a). Schematic representation of the PG plate as a base for inscription of integrated multi-purpose sensors and functional elements (b).

To further promote ultra-short laser applications such as barrier and integrated device inscription in volume of PGs, it is crucial to better control over both the required shape and morphology of the laser-modified region. Currently, a deep and well-controlled PG's densification is still challenging, particularly by a single laser pass and for the entire thickness of the sample. Nevertheless, high aspect ration modifications are required for faster fabrication of barriers, contrary to waveguides and channels (Fig. 1, b). The main open question is, therefore, how to better produce as deep and narrow densified regions as possible? For this the performance of the femtosecond laser treatment should be further improved by an appropriate choice of the optimum laser parameters.

Herein, we focus attention on ultra-short laser modifications induced in PG. In particular, we report ultra-short laser modifications induced in the bulk trying to determine optimum experimental conditions for the controllable three-dimensional laser writing of barriers in the bulk. To provide a better understanding of the physical mechanisms involved, both experiments and modeling are performed. Based on the obtained results, possibilities are proposed to increase the aspect-ratio of the densified regions by a particular choice of the laser-irradiation regime. The performed study is of interest for many potential applications, namely for laser fabrications of integrated sensors, molecular separators, bio-chambers, molecular machines, and waveguides.

Optical Materials EXPRESS

2. Experiments

In the experiments, 1 mm thick PG plates (0.30 Na_2O - 3.14 B_2O_3 - 96.45 SiO_2 - 0.11 Al_2O_3, mass fraction, %) [35]. The average pore radius is 4 nm at the porosity of 26%. The transparency of PG plates is high (≈90%) in visible and near IR ranges (0.2–2.5 μm), with the average refractive index $n \approx 1.34$ in the visible spectral range. Laser modification of PG samples was performed by a transverse volume scanning using femtosecond laser pulses with wavelength $\lambda = 515$ nm (second harmonic), pulse duration $\tau = 300$ fs, maximum pulse energy $E_p = 3\mu$J, operated in the TEM00 mode and at constant repetition rate of 500 kHz. Two lenses (10X, NA = 0.25 and 20X, NA = 0.4) were used to achieve laser beam waist diameter ($2\omega_0$) equal to 5.7μm or 3.6μm respectively.

After laser writing step, glass samples were polished at both facets for further investigation by optical microscopy (Carl Zeiss, Imager. A1m) in a transmission mode. Additionally, a linearly polarized light with a crossed polarizer/analyzer pair was used to investigate the birefringence form of fabricated structures. The cross-sectional samples were also prepared for scanning electron microscopy (SEM). The were covered by 2 – 5 nm carbon layer for the charge compensation. SEM images of the voids and channels were obtained by Carl Zeiss Merlin by using detectors of secondary and back-scattered electrons at accelerating voltage 20 kV and beam current equal to 1nA.

3. Results and discussion

3.1. Results of multi-pulse femtosecond laser scanning

For high repetition rate multi-pulse laser irradiation, the obtained results depend not only on laser pulse energy, E_p, but also on the number of laser pulses per laser spot, N. In this case, it is convenient to use the total incident laser energy, which is defined as follows $E_L = E_pN$. Thus, in the present study a series of ultra-short laser PG scanning were performed for two different focusing conditions by varying E_L. When E_L is small, porous glass densification is proven to take place [15,16,34] (Fig. 2(a). In the intermediate range of E_L, a series of voids are typically formed with a size up to ten micrometers (decompaction) (Fig. 2(b)). Further increase of E_L leads to the channel formation.

Here, we focus attention at the possibilities to obtain the deepest (the highest) possible PG densification. The focusing position was the same for all the cases, 300μm below the surface. For this, we firstly examine the shapes of the laser-modified zones, their heights (h) and widths (w), as presented as a function of E_L (Fig. 2). The obtained results show that when the lens with NA = 0.4 is used, only decompaction regime is observed (Fig. 2(a) and Fig. 2(b)). This regime is characterized by a big void formation at all the considered laser energies [15,16]. In this case, an increase in E_L leads to a more spherical laser-affected zone.

On the contrary, PG densification without void formation is possible if the total incident laser energy is below 7.5 mJ at NA = 0.25. Figures 2(c) and (d) demonstrate how the dimensions of the laser-densified volume evolve at NA = 0.25 as a function of laser energy. We note a considerable difference in the shape and energy-dependent behavior of the laser-affected volume: while the corresponding (w) increases both for NA = 0.4 and NA = 0.25, an increase in h is much more pronounced when NA is smaller.

Based on the obtained results for NA = 0.25, three different sub-regimes can be distinguished as follows:

(i) densification regime favorable for waveguide recording at E_L smaller than 2 mJ;

(ii) densification regime with a considerably increase the depth-to-width aspect ratio at E_L from 2 to 7.5 mJ;

(iii) decompaction regime at E_L higher than 7.5 mJ.

Optical Materials EXPRESS

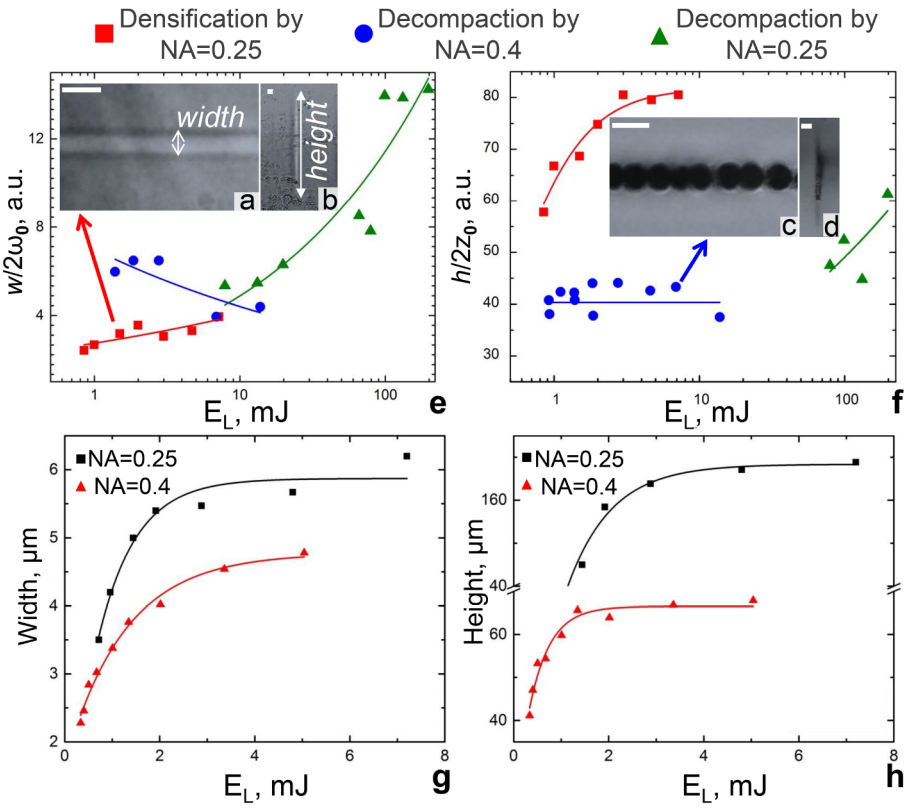

Fig. 2. Top view and cross-section microphotos of fabricated structures in PG: densification region (a,b) obtained by E_L = 2 mJ and 10X, NA = 0.25 lens, and voids (c,d) by E_L = 2 mJ and 20X, NA = 0.4 lens. Measured ratio of w to the laser beam waist diameter (e) for two lenses and h to the Rayleigh length ($2z_0$) (f) as a function of E_L. Experimental dependencies obtained for different NA: width (g) and height (h) of the modified region as a function of E_L. The scale bar is 10 μm.

We note that the second regime is more appropriate for barrier formation, where care should be taken to elongate the densified region in depth. The use of lenses with even smaller numerical aperture leads to an unacceptable broadening of the laser-affected zone.

Importantly, all the laser-induced tracks fabricated by laser scanning in the identified densification regime (NA = 0.25, the total incident laser energy from 0.8 mJ to 7.5 mJ) are characterized by the absence of voids or channel inside (Fig. 3(a,b)). Images taken in the polarized light also indicate an absence of the residual stress in the fabricated modification regions (Fig. 3(c)). We note that when NA = 0.4, heterogeneous regions were fabricated (Fig. 3(d)). SEM images confirm the presence of of nano- (200 – 300 nm) and micro-cavities (1 – 2μm) in the entire modification area (Fig. 3(e)). For instance, a luminous central core was observed in a linearly polarized light with a crossed polarizer/analyzer pair indicating the presence of stresses (Fig. 3(f)). Because neither voids nor stresses are desirable in the direct laser writing of embedded barriers, the use of lenses with smaller NA looks much more promising.

3.2. Single-pulse mechanism

The observed results rely on the physical processes involved in the formation of laser-induced modifications. When femtosecond laser is used, non-linear ionization generates electron plasma

Optical Materials EXPRESS

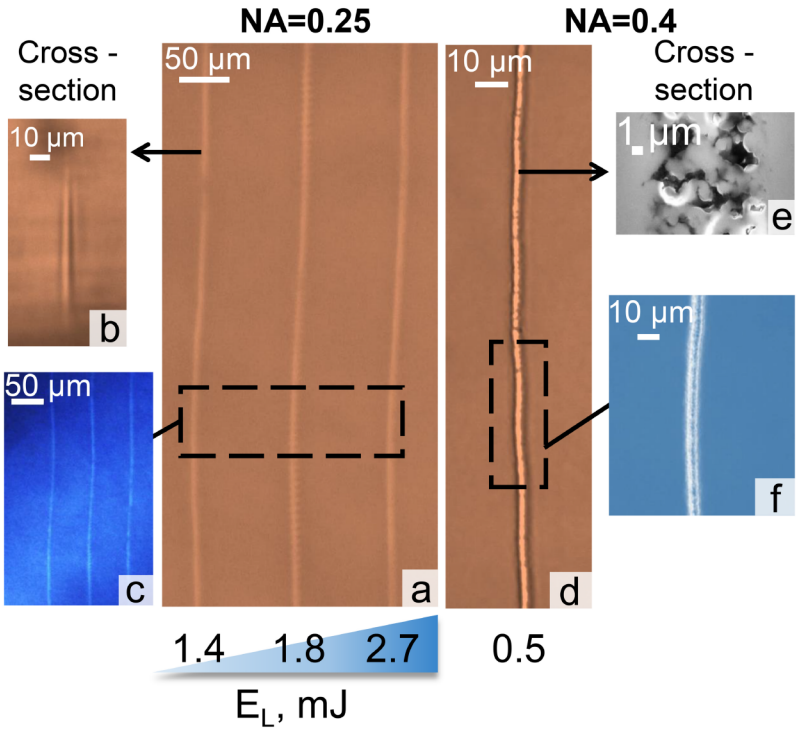

Fig. 3. Illustration of the difference in the application of two lenses: with NA = 0.25 (a-c) and 0.4 (d-f). Micro-images of laser-modified regions formed at constant $E_p = 1.8\mu$J and different N, where $E_L = 1.4, 1.8, 2.7$ mJ (a). Cross-section of the track formed at 1.4 mJ (b). Optical image of the densified tracks array in a linearly polarized light with a crossed polarizer/analyzer pair (c, f). SEM image of the track formed with NA=0.4 at $E_L = 0.5$ mJ (e).

(ELP). Both defect formation and ELP relaxation lead to the local modifications in the refractive index. As a result, optical properties, such as scattering and absorption, are modified.

The generated ELP strongly affects laser propagation. Our calculations [16] show that the maximum ELP density depends on both laser focusing conditions and laser pulse energy (Fig. 4(a)). Importantly, optical breakdown takes place at laser energy of 1.9μJ for NA = 0.25, whereas for NA = 0.4 it is expected at at a much smaller laser energy (0.7μ J). The transmission also drops at much smaller energy for NA = 0.4 than for NA = 0.25 ((Fig. 4(b)). These results explain the difference in the material modifications regimes observed for these two different laser focusing conditions. Importantly, if laser power is above the critical one $P_{cr} = 3.77\lambda^2/8\pi n_0 n_1$, where n_0 and n_1 stand for the linear (1.34) and nonlinear refractive ($\approx 0.4 \times 10^{-19} m^2/W$) indexes of the material [36], $P_{cr} = 7.4 \times 10^5 W$), the laser propagation of a Gaussian laser pulse is accompanied by such effects as self-focusing and filamentation [37]. Further increase in laser power becomes inefficient (a so-called "intensity clamping effect" [38]).

In all the experiments, laser power exceeded the critical one. In fact, $P_0 = E_p/\tau$, it ranges from $5.0 \times 10^5 W$ to $1.2 \times 10^7 W$ for E_p at $0.1\mu J$ and $2.3\mu J$ respectively. Despite the fact that the critical power does not depend on the laser focusing, both the characteristic length of the filament appearance z_f (1) and filament dimension strongly depends on the laser beam waist [37], where

$$z_f = \frac{0.367 k \omega_0^2}{\sqrt{[(P_0/P_{cr})^{1/2} - 0.852]^2 - 0.0219}} \quad (1)$$

Optical Materials EXPRESS

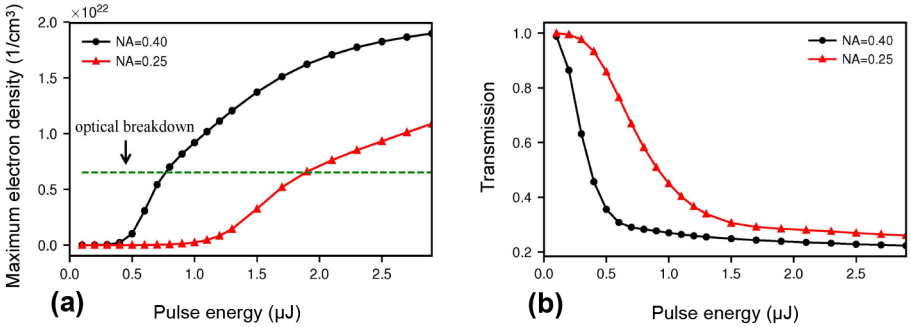

Fig. 4. Calculated maximum electron density (a) and light transmission (b) for single ultra-short laser pulse. The model parameters are given in [16].

where, k is a coefficient. Note that the equation would be invalid for incident power $P_0 > 100P_{cr}$ [37]. Because z_f is proportional to ω_0^2, even rather small difference in ω_0 affects the filamentation process. In our case, when NA = 0.25 ($2\omega_0 = 5.7\mu m$), and if NA = 0.4 ($2\omega_0 = 3.6\mu m$), so that the ratio of z_f parameter in our case is ≈ 2.5. This means that for NA = 0.25 laser propagates ≈ 2.5 longer distance before the possible appearance of self-focusing than at NA = 0.4. During the propagation path, the absorption and heating of ELP typically lead to laser energy losses. In fact, denser plasma formation and heating lead to the decompaction (void formation) rather than to the formation of a densified region. Thus, at smaller values of E_L, mostly densification is observed for NA = 0.25 (Fig. 2).

3.3. Multi-pulse heat accumulation

As we have noted in the Introduction, additional effects, such as defect, electronic and/or thermal accumulation, play a role in a multi-pulse regime. Particularly, heat accumulation depends on laser pulse width, repetition rate, laser spot dimensions and scanning speed, as well as on the material properties.

For this case, a combined model was developed [16] that carefully accounts for ultra-short laser light propagation, material ionization, and heating. A series of calculations are performed for the case of NA = 0.25 (Fig. 5). Based on the calculated temperature distributions (Fig. 5(a)), we evaluate the sizes of the laser-modified region (Fig. 5(b) and (c)). In the presented experiments discussed above, the system is designed to control the total incident laser energy E_L. To better compare the multi-pulse simulations with experiments, the results are shown as a function of E_L, which is calculated as $E_L = \frac{2\omega_0 f_p E_p}{Vs}$, where $f_p = 500kHz$ is the repetition rate, Vs is the laser scanning speed. The performed simulations reveal how the corresponding temperature profiles change with the increase in laser pulse energy for two laser scan speeds (1 mm/s and 45 mm/s). At high speed, a tail appears in the temperature distribution if laser pulse energy is high enough. This tail is commonly observed behind powerful moving heat sources. The higher the speed of the heat source, the longer is the tail. At lower laser energies, this tail is, however, less pronounced.

Importantly, Fig. 5 confirms the experimentally observed rise and saturation in the dimensions of the laser-modified area. Here, they were estimated based on the dimension of the region where temperature exceeds softening one. The observed saturation in the dimensions of laser-densified region is mainly caused by the reflection and scattering effects of the ELP.

We note, furthermore, that laser-induced modifications in local optical properties are known to cause local field enhancement [39,40] and pulse-to-pulse elongation of the laser-affected region. Upon many pulse, depending on laser energy, repetition rate, induced refractive index change, and the size of the modified area, such accumulation effects either lead to a further increase in the aspect ratio of the laser-modified region [41,42], or to the appearance of a big void in its center if

Optical Materials EXPRESS

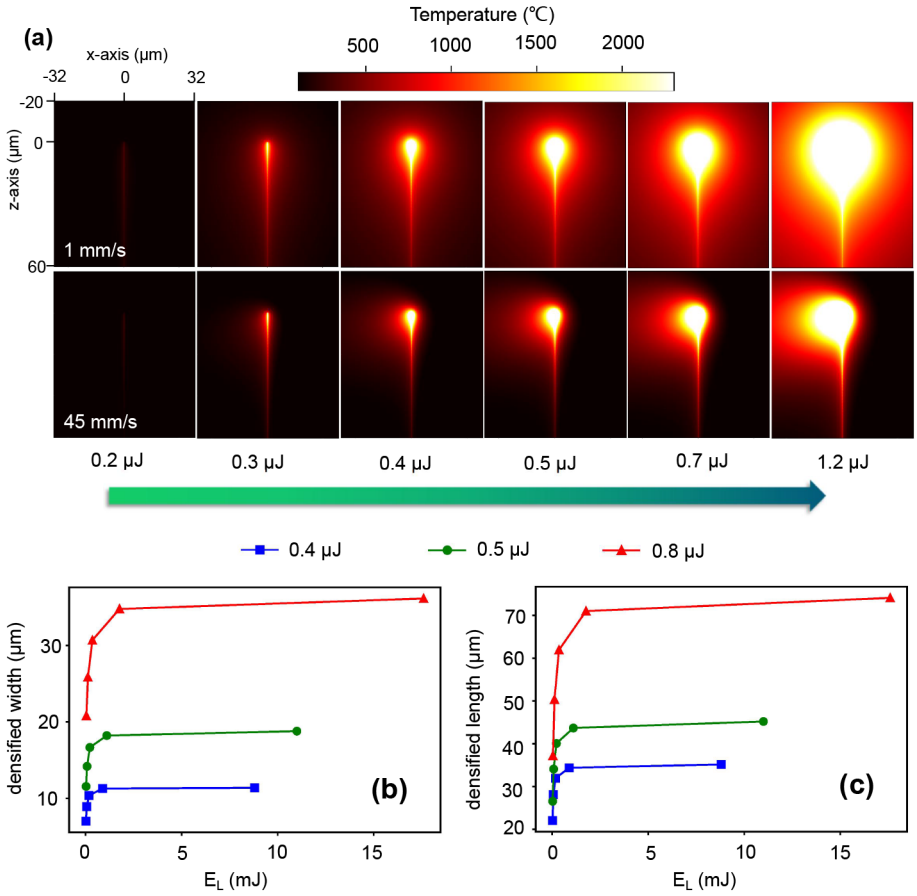

Fig. 5. Heat accumulation by an ultra-fast laser of high repetition-rate (500 kHz NA = 0.25) at various pulse energies and scanning speeds (a). Laser moves in the positive X direction (from left to right). Dimension of the densified area: width (b) and elongation (c). Here, these dimensions are estimated based on the temperature of 1000°C [15].

laser energy is high enough [11,15,22]. It is estimated that about $2.5\mu J$ per pulse is required the void formation [16,22].

4. Toward efficient laser writing of barriers in PG

As we have noted above, laser writing of barriers is a promising application of the high-aspect ratio porous glass densification since it provides a way to locally control over molecular permeability. For this, as discussed above, the regime with NA = 0.25 and pulse energy smaller $1\mu J$ are preferable. Even with these parameters, however, to cover $500\mu m$ thickness, our recording procedure included two steps: (i) femtosecond laser recording of 4 tracks forming a barrier through the entire depth of the glass plate; and (ii) 2 tracks on the surface of PG written with CO_2 laser radiation for a complete sealing of the barrier [34]. Schematic view and micro-photo are shown in Fig. 6(a, b).

As shown above, the single-step track height is limited to around $165\mu m$ in the initial PG (Fig. 2, d). In this section, we demonstrate how the aspect ratio of the densified zone can be further increased allowing much longer barrier recording in a single step. In fact, we propose to

Optical Materials EXPRESS

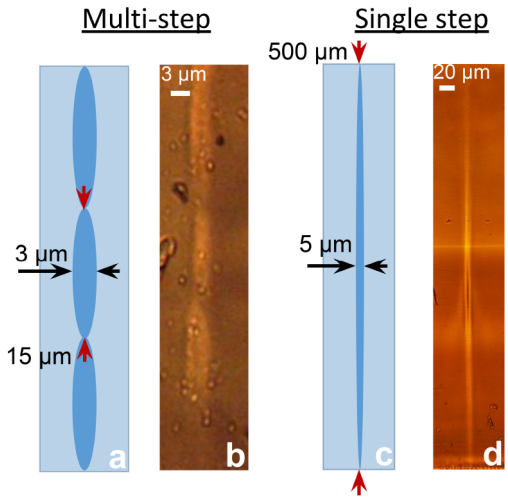

Fig. 6. Cross-section schematic view of the barrier fabrication in PG: multi-step densification by 3 scans with the track height of 15μm provides the barrier height of 45μm (a) and its micro-photo (b); the 500μm-barrier fabricated by 1 femtosecond laser track inside of water doped PG plate with thickness of 500μm (c). Micro-photo of thought barrier inside of PG (d).

further extend the filament length induced by the femtosecond laser in PG with plate thickness of 500μm.

It should be noted that parameters, such as optical breakdown threshold, size and peak intensity of the filament, strongly depend on the optical characteristics of the propagation medium [37]. PG samples contain pores leading to a considerable Rayleigh scattering. Filling or doping of these pores is known to modify both ultra-short laser propagation and laser processing results. For instance, porous glass doping by NaCl was shown not only to reduce the threshold fluence of optical breakdown, but also to facilitate volume nanograting formation with shorter periods [43]. Water-assisted femtosecond laser direct writing also provided opportunities to develop novel 3D micro-nanofluidic systems for a variety of lab-on-a-chip applications [44].

Herein, we fill our PG glass with water to obtain a more homogeneous medium thus extending the length of the filament. The use of water also allows us to significantly increase the range of laser power densities for the PG densification process. Thus, the permitted energy per pulse increases by at least 15 %.

Figure 6, d demonstrates that the presence of water indeed leads to an increase in the filament length up to 500μm. The laser recording of such high-aspect ratio dandified barrier is carried out using a high-aperture objective lens 20x, NA = 0.4, at which the areas of decompaction were also formed in PG without water (Fig. 3, d). In this case, only one scan in such filamentation mode is enough to create a barrier through the entire thickness of the glass plate.

5. Conclusion

To summarize, we have investigated ultra-short laser interaction with PG in a high repetition rate multi-pulse regime. Conditions favorable for the inscription of either highly symmetric wave-guides or high aspect-ratio membrane and barriers are determined. For this, the effects of the change in laser energy and focusing conditions on the material modifications are examined. The performed experiments have revealed considerable differences in the dimensions of the laser-modified zone, and particularly, in their dependency on laser energy. For NA = 0.25,

Optical Materials EXPRESS

the modified area was either very prolonged and densified, or was found to be more and more spherical when a void was formed in its center. For NA = 0.4, only decompaction, or a large void formation was observed in the considered laser irradiation regime with the length that was practically independent on E_L, whereas the diameter was found to slightly decay with E_L. Thus, we have not only identified the preferable regime for void-free material densification, but have also discriminated between two possible densification sub-regimes revealed for NA = 0.25.

The observed difference was explained based on a series of numerical calculations. Laser focusing affects filament appearance distance. In the considered case, this effect is minor compared to the effect of the laser-induced ionization since the created ELP strongly affects thermal field as well as the shape of the laser-affected zone. The characteristic dimensions of the calculated temperature field are well correlated with the obtained shapes of the densified regions. The maximum density of the created electron plasma was found, furthermore, to strongly depend on the focusing conditions.

In the case of the porous glass filled with air, however, the height of the densified volume is limited to $165\mu m$. We have demonstrated that filling of the PG with water allows a considerable increase in the filament length up to $500\mu m$.

Laser-based high aspect ratio densification is promising for numerous applications in microfluidics and for the fabrication of the integrated multi-purpose sensors. The identified laser irradiation conditions required for the efficient void-free material densification thus provide a way toward a better control over direct laser writing of membranes, barriers and various integrated devices in porous glasses.

Funding

Campus France (38091TJ).

Acknowledgments

H.M is grateful to The French Ministry of Science and Education for his PhD Scholarship. ITMO Professorship and Fellowship program is gratefully acknowledged. R.Z. is grateful to Avesta Ltd. for the opportunity to work with the femtosecond laser.

References

1. R. Osellame, G. Cerullo, and R. Ramponi, *Femtosecond Laser Micromachining: Photonic and Microfluidic Devices in Transparent Materials*, vol. 123 (Springer Science & Business Media, 2012).
2. R. R. Gattass and E. Mazur, "Femtosecond laser micromachining in transparent materials," Nat. Photonics **2**(4), 219–225 (2008).
3. F. Korte, J. Serbin, J. Koch, A. Egbert, C. Fallnich, A. Ostendorf, and B. Chichkov, "Towards nanostructuring with femtosecond laser pulses," Appl. Phys. A: Mater. Sci. Process. **77**, 229–235 (2003).
4. K. Sugioka, Y. Hanada, and K. Midorikawa, "Three-dimensional femtosecond laser micromachining of photosensitive glass for biomicrochips," Laser Photonics Rev. **4**(3), 386–400 (2010).
5. J. Serbin, A. Egbert, A. Ostendorf, B. Chichkov, R. Houbertz, G. Domann, J. Schulz, C. Cronauer, L. Fröhlich, and M. Popall, "Femtosecond laser-induced two-photon polymerization of inorganic–organic hybrid materials for applications in photonics," Opt. Lett. **28**(5), 301–303 (2003).
6. Z. Chaboyer, T. Meany, L. Helt, M. J. Withford, and M. Steel, "Tunable quantum interference in a 3D integrated circuit," Sci. Rep. **5**(1), 9601 (2015).
7. M. Malinauskas, A. Žukauskas, S. Hasegawa, Y. Hayasaki, V. Mizeikis, R. Buividas, and S. Juodkazis, "Ultrafast laser processing of materials: from science to industry," Light: Sci. Appl. **5**(8), e16133 (2016).
8. K. Sugioka and Y. Cheng, "Ultrafast lasers-reliable tools for advanced materials processing," Light: Sci. Appl. **3**(4), e149 (2014).
9. A. Rudenko, J.-P. Colombier, and T. E. Itina, "Nanopore-mediated ultrashort laser-induced formation and erasure of volume nanogratings in glass," Phys. Chem. Chem. Phys. **20**(8), 5887–5899 (2018).
10. M. Ams, P. Dekker, S. Gross, and M. J. Withford, "Fabricating waveguide bragg gratings (WBGS) in bulk materials using ultrashort laser pulses," Nanophotonics **6**(5), 743–763 (2017).
11. W. Watanabe, T. Toma, K. Yamada, J. Nishii, K.-i. Hayashi, and K. Itoh, "Optical seizing and merging of voids in silica glass with infrared femtosecond laser pulses," Opt. Lett. **25**(22), 1669–1671 (2000).

Optical Materials EXPRESS

12. C. Liu, Y. Liao, F. He, Y. Shen, D. Chen, Y. Cheng, Z. Xu, K. Sugioka, and K. Midorikawa, "Fabrication of three-dimensional microfluidic channels inside glass using nanosecond laser direct writing," Opt. Express **20**(4), 4291–4296 (2012).
13. Y. Bellouard, A. Champion, B. McMillen, S. Mukherjee, R. R. Thomson, C. Pépin, P. Gillet, and Y. Cheng, "Stress-state manipulation in fused silica via femtosecond laser irradiation," Optica **3**(12), 1285–1293 (2016).
14. F. He, H. Xu, Y. Cheng, J. Ni, H. Xiong, Z. Xu, K. Sugioka, and K. Midorikawa, "Fabrication of microfluidic channels with a circular cross section using spatiotemporally focused femtosecond laser pulses," Opt. Lett. **35**(7), 1106–1108 (2010).
15. V. P. Veiko, S. I. Kudryashov, M. M. Sergeev, R. A. Zakoldaev, P. A. Danilov, A. A. Ionin, T. V. Antropova, and I. N. Anfimova, "Femtosecond laser-induced stress-free ultra-densification inside porous glass," Laser Phys. Lett. **13**(5), 055901 (2016).
16. H. Ma, R. A. Zakoldaev, A. Rudenko, M. M. Sergeev, V. P. Veiko, and T. E. Itina, "Well-controlled femtosecond laser inscription of periodic void structures in porous glass for photonic applications," Opt. Express **25**(26), 33261–33270 (2017).
17. J. Bonse, S. Baudach, J. Krüger, W. Kautek, and M. Lenzner, "Femtosecond laser ablation of silicon–modification thresholds and morphology," Appl. Phys. A **74**(1), 19–25 (2002).
18. T. J.-Y. Derrien, J. Krüger, T. E. Itina, S. Höhm, A. Rosenfeld, and J. Bonse, "Rippled area formed by surface plasmon polaritons upon femtosecond laser double-pulse irradiation of silicon: the role of carrier generation and relaxation processes," Appl. Phys. A **117**(1), 77–81 (2014).
19. B. Luther-Davies, A. V. Rode, N. R. Madsen, and E. G. Gamaly, "Picosecond high-repetition-rate pulsed laser ablation of dielectrics: the effect of energy accumulation between pulses," Opt. Eng. **44**(5), 051102 (2005).
20. O. Uteza, B. Bussiere, F. Canova, J.-P. Chambaret, P. Delaporte, T. Itina, and M. Sentis, "Laser-induced damage threshold of sapphire in nanosecond, picosecond and femtosecond regimes," Appl. Surf. Sci. **254**(4), 799–803 (2007).
21. C. B. Schaffer, J. F. García, and E. Mazur, "Bulk heating of transparent materials using a high-repetition-rate femtosecond laser," Appl. Phys. A **76**(3), 351–354 (2003).
22. N. M. Bulgakova, V. P. Zhukov, S. V. Sonina, and Y. P. Meshcheryakov, "Modification of transparent materials with ultrashort laser pulses: What is energetically and mechanically meaningful?" J. Appl. Phys. **118**(23), 233108 (2015).
23. I. Miyamoto, K. Cvecek, Y. Okamoto, and M. Schmidt, "Internal modification of glass by ultrashort laser pulse and its application to microwelding," Appl. Phys. A **114**(1), 187–208 (2014).
24. C. Momma, S. Nolte, B. N. Chichkov, F. V. Alvensleben, and A. Tünnermann, "Precise laser ablation with ultrashort pulses," Appl. Surf. Sci. **109-110**, 15–19 (1997).
25. Y. Li, K. Itoh, W. Watanabe, K. Yamada, D. Kuroda, J. Nishii, and Y. Jiang, "Three-dimensional hole drilling of silica glass from the rear surface with femtosecond laser pulses," Opt. Lett. **26**(23), 1912–1914 (2001).
26. S. M. Eaton, H. Zhang, P. R. Herman, F. Yoshino, L. Shah, J. Bovatsek, and A. Y. Arai, "Heat accumulation effects in femtosecond laser-written waveguides with variable repetition rate," Opt. Express **13**(12), 4708–4716 (2005).
27. S. Richter, S. Döring, F. Burmeister, F. Zimmermann, A. Tünnermann, and S. Nolte, "Formation of periodic disruptions induced by heat accumulation of femtosecond laser pulses," Opt. Express **21**(13), 15452–15463 (2013).
28. P. S. Salter, M. Baum, I. Alexeev, M. Schmidt, and M. J. Booth, "Exploring the depth range for three-dimensional laser machining with aberration correction," Opt. Express **22**(15), 17644–17656 (2014).
29. S. M. Eaton, H. Zhang, M. L. Ng, J. Li, W.-J. Chen, S. Ho, and P. R. Herman, "Transition from thermal diffusion to heat accumulation in high repetition rate femtosecond laser writing of buried optical waveguides," Opt. Express **16**(13), 9443–9458 (2008).
30. T. Tanaka, T. Ohyama, Y. Y. Maruo, and T. Hayashi, "Coloration reactions between NO_2 and organic compounds in porous glass for cumulative gas sensor," Sens. Actuators, B **47**(1-3), 65–69 (1998).
31. Y. Y. Maruo and J. Nakamura, "Portable formaldehyde monitoring device using porous glass sensor and its applications in indoor air quality studies," Anal. Chim. Acta **702**(2), 247–253 (2011).
32. S. Ding, C. Gao, and L.-Q. Gu, "Capturing single molecules of immunoglobulin and ricin with an aptamer-encoded glass nanopore," Anal. Chem. **81**(16), 6649–6655 (2009).
33. J. Zhang, A. Čerkauskaitė, R. Drevinskas, A. Patel, M. Beresna, and P. G. Kazansky, "Eternal 5D data storage by ultrafast laser writing in glass," in *Laser-based Micro-and Nanoprocessing X*, vol. 9736 (International Society for Optics and Photonics, 2016), p. 97360U.
34. V. P. Veiko, R. A. Zakoldaev, M. M. Sergeev, P. A. Danilov, S. I. Kudryashov, G. K. Kostiuk, A. N. Sivers, A. A. Ionin, T. V. Antropova, and O. S. Medvedev, "Direct laser writing of barriers with controllable permeability in porous glass," Opt. Express **26**(21), 28150–28160 (2018).
35. V. Kreisberg and T. Antropova, "Changing the relation between micro-and mesoporosity in porous glasses: The effect of different factors," Microporous Mesoporous Mater. **190**, 128–138 (2014).
36. J. Cimek, N. Liaros, S. Couris, R. Stepień, M. Klimczak, and R. Buczyński, "Experimental investigation of the nonlinear refractive index of various soft glasses dedicated for development of nonlinear photonic crystal fibers," Opt. Mater. Express **7**(10), 3471–3483 (2017).
37. A. Couairon and A. Mysyrowicz, "Femtosecond filamentation in transparent media," Phys. Rep. **441**(2-4), 47–189 (2007).
38. Z. Xu, W. Liu, N. Zhang, M. Wang, and X. Zhu, "Effect of intensity clamping on laser ablation by intense femtosecond laser pulses," Opt. Express **16**(6), 3604–3609 (2008).

Optical Materials EXPRESS

39. A. Pereira, D. Grojo, M. Chaker, P. Delaporte, D. Guay, and M. Sentis, "Laser-fabricated porous alumina membranes for the preparation of metal nanodot arrays," Small **4**(5), 572–576 (2008).
40. M. Rasedujjaman and L. Gallais, "Polarization dependent laser damage growth of optical coatings at sub-picosecond regime," Opt. Express **26**(19), 24444–24460 (2018).
41. A. Rudenko, J.-P. Colombier, and T. E. Itina, "From random inhomogeneities to periodic nanostructures induced in bulk silica by ultrashort laser," Phys. Rev. B **93**(7), 075427 (2016).
42. E. Mcleod and C. B. Arnold, "Subwavelength direct-write nanopatterning using optically trapped microspheres," Nat. Nanotechnol. **3**(7), 413–417 (2008).
43. F. A. Umran, Y. Liao, M. M. Elias, K. Sugioka, R. Stoian, G. Cheng, and Y. Cheng, "Formation of nanogratings in a transparent material with tunable ionization property by femtosecond laser irradiation," Opt. Express **21**(13), 15259–15267 (2013).
44. Y. Cheng, Y. Liao, and K. Sugioka, "Laser-induced damage in porous glass: a pathway to 3D fabrication of micro-/nanofluidics," in *Pacific Rim Laser Damage 2013: Optical Materials for High Power Lasers*, vol. 8786 (International Society for Optics and Photonics, 2013), p. 87860C.